Paper 025

# THE DEVELOPMENT OF A LARGE CIVIL TILTROTOR SIMULATION FOR HOVER AND LOW-SPEED HANDLING QUALITIES INVESTIGATIONS


Ben Lawrence
NASA Postdoctoral Program Fellow
Ames Research Center
Moffett Field, CA, USA
Ben.lawrence@nasa.gov

Carlos A. Malpica
Colin R. Theodore
NASA
Ames Research Center
Moffett Field, CA, USA



## ABSTRACT

The NASA Subsonic Rotary Wing project is conducting research to radically improve the capabilities and civil benefits of rotary-wing vehicles and enhance mobility in the future air transportation system. Previous research has identified the Large Civil Tiltrotor 2 concept as the configuration with the best potential to meet the future requirements. However, there are many questions on what the flight dynamic, control, and handling qualities characteristics should be for such a large tiltrotor. Building on a research campaign of the LCTR2 hover and low speed handling qualities, this paper presents the development of a real-time simulation model designed for piloted handling qualities experiments. This includes how a qLPV or 'stitched' modeling approach that combines multiple linear stability derivative-based state-space models was successfully used to provide varying model dynamics and trim characteristics for changing flight speed and nacelle angle. Finally, it will be described how the qLPV model was integrated into a control architecture that featured Translational Rate Control using nacelle and lateral cyclic as the primary effectors. Finally, the paper shall describe how the combined airframe-control system model was successfully integrated into the NASA Vertical Motion Simulator and adjudged fit for the purpose of hover and low speed piloted handling qualities experiments.


## 1. NOMENCLATURE

| | |
|---|---|
| $\vec{a}$ | Body Axes linear Acceleration Vector |
| $\mathbf{A}$ | State Matrix |
| $\mathbf{B}$ | Control Matrix |
| c | Blade Chord |
| $C_{l_\alpha}$ | Lift Curve Slope |
| $g$ | Acceleration Due to Gravity |
| $I$ | Inertia Tensor |
| $I_{yy}$ | Pitch Moment of Inertia (slug-ft^2) |
| $m$ | Mass |
| $M_w$, $Z_q$ | Stability Derivatives in Concise Notation i.e. $M_w = \frac{\partial M}{\partial w}\left(\frac{1}{I_{yy}}\right), Z_q = \frac{\partial Z}{\partial q}\left(\frac{1}{m}\right)$ |
| $N_b$ | Number of Blades |
| $p$, $q$, $r$ | Angular Rates About the Body X,Y and Z Axes. |
| $\vec{r}_{N/F}$ | Position vector of nacelle system center of mass with respect to fuselage center of mass |
| R | Radius of Rotor |
| $S1M1C$ | Symmetric Longitudinal Flapping |
| $S(\vec{\omega})$ | Skew symmetric tensor representing vector cross product linear transformation |
| $T$ | Rotor Thrust |
| $u$, $v$, $w$ | Body X, Y and Z Axes Velocities |
| $\mathbf{u}$ | Control Vector |
| $U_0$ | Trim Body X-axis Velocity |
| $V$ | Speed in Body Axes X-X Plane |
| $\vec{V}$ | Body Axes Linear Velocity Vector |
| $\mathbf{x}$ | State Vector |
| $X_H, Z_H$ | X,Z Rotor Forces in Hub Frame |
| $x_H$, $z_H$ | Longitudinal and vertical position in body frame of rotor hub with respect to aircraft body reference frame center |
| $Z_0$ | Equilibrium or Trim Z-Force |
| $\alpha$ | Angle of Attack |


*Presented at the 36th European Rotorcraft Forum, Paris, France, Sept 7-9, 2010.*

| | |
|---|---|
| $\vec{\alpha}$ | Body Axes Angular Acceleration Vector |
| $\beta_m$ | Nacelle Angular Displacement (Mast Conversion Angle) |
| $\dot{\beta}_m$ | Nacelle Angular Rate |
| $\ddot{\beta}_m$ | Nacelle Angular Acceleration |
| $\delta Z$ | Perturbation in Z-Force |
| $\Delta \dot{v}_g$ | Perturbation in Body Axis Acceleration due to Gravity |
| $\frac{\partial Z}{\partial \ddot{\beta}_m}$ | Aircraft Body Axis Z-force due Nacelle Angular Acceleration |
| $\frac{\partial Z}{\partial \dot{\beta}_m}$ | Aircraft Body Axis Z-force due Nacelle Angular Rate |
| $\frac{\partial Z}{\partial \beta_m}$ | Aircraft Body Axis Z-force due Nacelle Angular Displacement |
| $\lambda_i$ | Rotor Induced Inflow |
| $\mu_x$ | Advance Ratio in Hub Frame X-axis |
| $\rho$ | Density of Air |
| $\theta, \varphi$ | Pitch, Roll Euler Angles |
| $\theta_0$ | Collective Angle |
| $\theta_{1s}$ | Longitudinal Cyclic |
| $\theta_{tw}$ | Blade Linear Twist |
| $\rho_k$ | qLPV Model Lookup Variable |
| $\Delta$ | Perturbation |
| $\Omega$ | Rotorspeed |

***Subscripts***

| | |
|---|---|
| *B* | Body Axes |
| *0* | Trim or Equilibrium |
| *N* | Nacelle (i.e. $m_N$, Nacelle mass) |
| $N/_F$ | Nacelle Dynamics with Respect to Fuselage Reference Frame |
| *F* | Fuselage |
| *H* | Hub Axes |
| *m* | Mast (i.e. $\beta_m$ is mast angle = nacelle angle) |
| *n, i* | Number of States, *i=1* →*n* |
| *p, j* | Number of Controls, *j=1* →*p* |
| *k* | k-th qLPV Model Lookup/Scheduling Variable |

## 2. INTRODUCTION

### 2.1 BACKGROUND

NASA's Subsonic Rotary Wing (SRW) project, part of the Fundamental Aeronautics Program (www.aeronautics.nasa.gov/fap), conducts research to radically improve the capabilities and civil benefits of rotary-wing vehicles and enhance mobility in the future air transportation system. The research effort to increase speed and range, payload, propulsive efficiency and to reduce noise has promoted the development of rotorcraft configurations such as large size, heavy lift tiltrotors for a future VTOL civil transport vehicle.

The goal is to meet future requirements tied to the vision of the Next Generation Air Transportation System (NextGen) www.faa.gov/nextgen, such as increasing capacity and reducing congestion at airports. NASA conducted the Heavy Lift Rotorcraft Systems Investigation, an in-depth multidisciplinary study which examined several large civil transport rotorcraft configurations [1].

The Large Civil Tiltrotor concept was identified as the configuration with the best potential to meet the future requirements. The design has been refined to the LCTR2 (Large Civil TiltRotor, 2nd generation) which NASA has adopted as the concept vehicle for programs aimed at technology risk reduction for such aircraft [2]. The LCTR2 is designed for the short-haul regional market and to carry 90 passengers over a range of at least 1000nm at 300kts. The layout of the LCTR2 is illustrated in Figure 1. The key features include twin contra-rotating 65ft (19.8m) diameter proprotors, 107ft (32.6m) wingspan with tilting wing tip sections and 'V' tail surfaces. The baseline gross weight is 103,600lb (47,000kg). Ref [2] can be consulted for a full description of the LCTR2 design evolution.

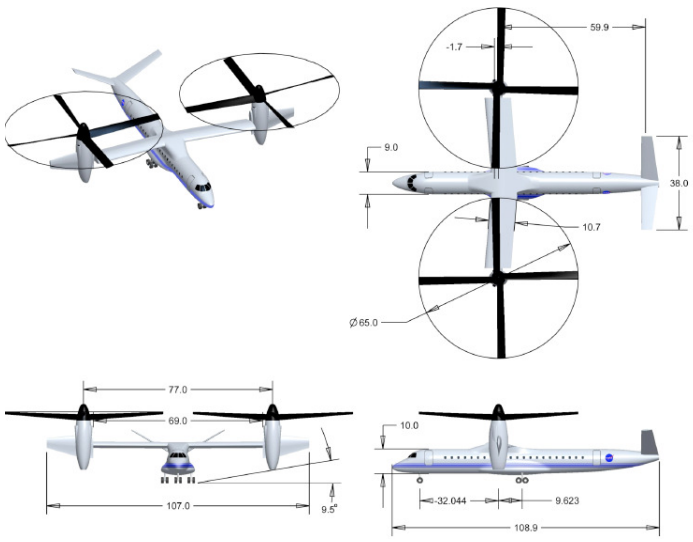


**Figure 1: NASA Large Civil Tiltrotor (LCTR2)**

### 2.2 FLIGHT CONTROL RESEARCH WITH LCTR2

Naturally, there are many questions on what the flight dynamic, control, and handling qualities characteristics

should be for such a large tiltrotor. Initial piloted simulation investigations in the NASA Ames Vertical Motion Simulator (VMS) showed that control in hover posed some "interesting challenges". As a result, subsequent experiments primarily concentrated their efforts on a systematic investigation of the fundamental handling qualities of a LCTR2-sized tiltrotor in hover. The first of these focused on stability margins and disturbance rejection bandwidth of the feedback control laws, whilst the second investigated the effect of the aircraft bandwidth and phase delay characteristics on the fundamental attitude response handling qualities [3],[4].

For these previous experiments, single-point (i.e. hover) stability derivative state-space models were used. These were generated from a high fidelity model in the CAMRAD II comprehensive rotorcraft aeromechanics analysis code. The linear models were reduced in order and the longitudinal and lateral dynamics were decoupled. These bare-airframe models were then augmented with a model-following Attitude Command, Attitude Hold (ACAH) control system [4]. Models of this fidelity were deemed adequate for the assessment of the fundamental attitude flight dynamics in the ADS-33 Precision Hover and Hover Turn tasks [5].

To carry the research forward, there were two new main requirements: The first was to provide a model with an expanded flight envelope to be valid up to 60kts forwards and ±40kts laterally to provide representative dynamics (including full inter-axes coupling) in the ADS-33 Lateral Reposition and Depart/Abort handling qualities maneuvers [5]. To meet this requirement, a Linear Parameter Varying (LPV) modeling approach [6] was chosen to develop a model of the LCTR2 suitable for the real-time simulation piloted handling qualities experiments. This paper describes the model architecture devised and the processes of extracting the input data and configuring the models, as well as an initial assessment of the model performance.

The second key requirement was to provide nacelle tilt and rotor lateral cyclic control. Although nacelle tilt is primarily for a tiltrotor's high speed cruise mode it also is a useful control in hover and low speed. The nacelles can be used to generate forward velocities whilst maintaining a level pitch attitude of the aircraft. This mode of operation is already typical of tiltrotor aircraft where the pilot is able to control the nacelle angle directly. However, this model enables the use of the nacelles in a closed loop controller. In this paper, a description is provided of how this active form of nacelle control, in conjunction with parallel lateral cyclic inputs (tilting of the rotor discs in the same direction laterally), is used to provide Translational Rate Control (TRC) in the longitudinal and lateral axes.

The addition of nacelle kinematics brought a number of challenges, especially as the baseline CAMRAD II model, although able to provide linear models at fixed nacelle angles, was unable to provide models that included effects due to nacelle motion itself. These effects had to be incorporated by other means and it will be discussed how this was achieved using alternate models and analytical techniques. Finally, a description of the bare-airframe LPV model integration into the ACAH/TRC control architecture, and preliminary testing in piloted real-time simulation in preparation for the VMS experiment will be presented.

## 3. LINEAR PARAMETER VARYING MODELING

### *3.1 THEORY*

The LPV technique consists of 'stitching' together multiple stability derivative-based linear state-space models extracted from a range of trimmed flight conditions. The model stability derivatives are interpolated through lookup tables that are function of flight states (i.e. flight speed), control inputs or other configuration parameters. The expression in equation 1 illustrates that the formulation is an extension of the standard state space model [6]:

$$\dot{\mathbf{x}}(t) = \mathbf{A}(\rho_k)\Delta\mathbf{x}(t) + \mathbf{B}(\rho_k)\Delta\mathbf{u}(t) \qquad \textbf{(1)}$$

Here, $\rho_k$ are the lookup table independent variable(s), and may vary with time. There is no theoretical limit to how many lookup variables you can use as indicated by the subscript, *k*. The coefficients of the state and control matrices, $\mathbf{A}$ and $\mathbf{B}$ respectively, are a function of $\rho_k$ .

The state space formulation is based on the premise that any dynamics are a small perturbation from a datum, or in the case of flight vehicles, a trim condition. However, the simulation was required to represent more than perturbation effects including effects such as realistic trim changes in the controls and states with flight condition. So equation 1 is recast in the following way:

$$\dot{\mathbf{x}} = \mathbf{A}(\rho_k)\left(\mathbf{x} - \mathbf{x}_0(\rho_k)\right) + \mathbf{B}(\rho_k)\left(\mathbf{u} - \mathbf{u}_0(\rho_k)\right) \qquad \textbf{(2)}$$

Here, $\mathbf{x_0}(\rho_k)$ and $\mathbf{u_0}(\rho_k)$ are respectively the vectors of the trim states and controls at each of the reference conditions $\rho_k$ and are also interpolated from lookup tables. In this formulation $\mathbf{x}$ and $\mathbf{u}$ are the absolute values of the states and controls and thus the difference between these and the trim values is the perturbation value: $\Delta\mathbf{x} = \mathbf{x} - \mathbf{x}_0(\rho_k)$. Note that when the difference is zero, the vehicle has zero resultant accelerations, ($\dot{x} = 0$), and therefore will be in trim with the appropriate values of states and controls.

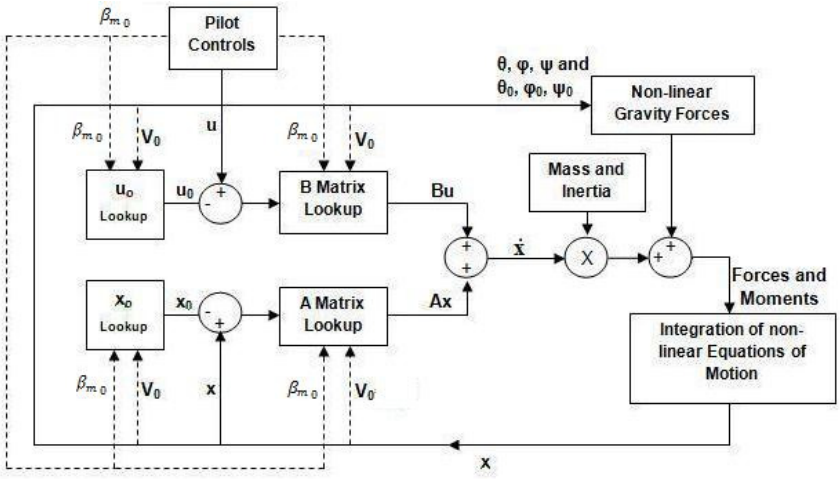


**Figure 2: Architecture for LCTR2 qLPV model**

### *3.2 IMPLEMENTATION*

The primary modeling tool for the LCTR2 LPV model was the MATLAB/Simulink environment. Figure 2 illustrates the architecture employed for the LCTR2 LPV model. It is first important to point out that the state space formulation **Ax + Bu** is only applied to the aerodynamic/propulsive force and moment contributions – i.e. all the linearized gravity (e.g. $g\theta$) are eliminated from the matrices and other inertial terms removed from the stability derivative terms (e.g. $Z_q$=$Z_q$ - $U_0 q$).

These gravity and inertial/coriolis effects are accounted for separately in the blocks labeled 'Non-linear gravity forces' and 'Integration of non-linear equations of motion'. In the gravitational force subsystem, the equations are the full nonlinear gravitational terms. However, these equations subtract the steady state force due to gravity as there is no representation of the aerodynamic trim forces in the model to counterbalance. This is achieved by inputting to this block the current absolute Euler angles and the 'looked-up' trim Euler angles and computing the terms twice using both angles and subtracting one from another to get the effective 'perturbation' due to the non-linear gravitational force. For example, for the lateral body axes equation:

$$\Delta\dot{v}_g = g\begin{pmatrix} cos(\theta)sin(\varphi) \\ -cos(\theta_0)sin(\varphi_0) \end{pmatrix} \quad \textbf{(3)}$$

So, if the aircraft is at the trim Euler angles, the resultant gravitational force is zero.

As shown in Figure 2, the resultant forces and moments due to the aerodynamic and propulsive effects are obtained by multiplying the translational and rotational accelerations by

the appropriate mass and inertia terms (which must be consistent with those used at the time of the extraction of the derivatives). These are then summed with the gravitational forces before being reconverted to accelerations for integration via standard Euler nonlinear equations of motion.

The final item to draw attention to is related to the lookup tables, which have their input parameters indicated by the dashed lines in Figure 2. For the LCTR2 model, the datum (trim) airspeed, $V_0$, and nacelle angle, $\beta_{m_0}$, were selected for the lookup table independent parameters (scheduling parameters). Airspeed is typically used as a scheduling parameter in LPV models of aircraft, as indicated in numerous papers ([6], [7], [8] and [9]). However, for a tiltrotor qLPV model, nacelle angle must also be considered in order to realistically capture the changing dynamics and trim. Another aspect of LPV modeling technique that has been followed for this model is the application of a low-pass filter on the lookup table scheduling parameters. In Ref [7] described how this approach was applied to the flight speed scheduling parameter and this techniques has been followed for this model.

At this instant, it is pertinent to highlight the difference in nature between the two 'lookup' parameters, $V_0$ and $\beta_{m_0}$, and to introduce certain nomenclature used in conjunction with LPV modeling. Firstly, they differ in that $V_0$, unlike $\beta_{m_0}$, is a state of the system (actually it is a combination of the u and w states as V is the resultant magnitude in the X-Z plane). As will be shown later, this 'endogenous' nature has important ramifications for the implementation of LPV models where a scheduling (lookup) parameter is also a state of the system and is usually defined as 'quasi-LPV' or qLPV [6]. In this case, the 'quasi' term refers to the fact that a nonlinear feedback of the state dependency could occur, meaning that system behavior may not be strictly linear. $\beta_{m_0}$ however, is exogenous, in that its value is entirely derived from the external pilot input and thus does not possess the same input/output dependency.

As indicated earlier, the baseline for the development of the real-time capable qLPV model was a high fidelity model of the LCTR2 constructed in the CAMRAD II comprehensive analysis code. This model features finite element, elastic beam, rotor blade models, a 3-state linear inflow model and

dynamic stall effects. CAMRAD II is a code optimized for trim, performance and aeromechanics analyses and is not designed to support real-time simulation. However, it does have a capability to extract **A**, **B**, **C** and **D** Jacobian matrices of the stability derivatives producing a linear, 110-state state-space model of the coupled rotor-body dynamics. As the model's purpose was primarily for handling qualities and flight dynamic analyses a reduced order of 13-state model was adjudged to be sufficient to accurately capture the dynamics important for flight control and handling quality analyses and real-time simulation. This consisted of the six-degree-of-freedom rigid body states (9 states) and 4 rotor states (1st order longitudinal and lateral flapping for the left and right rotors). The model order reduction was carried out using the MATLAB 'modred' function.

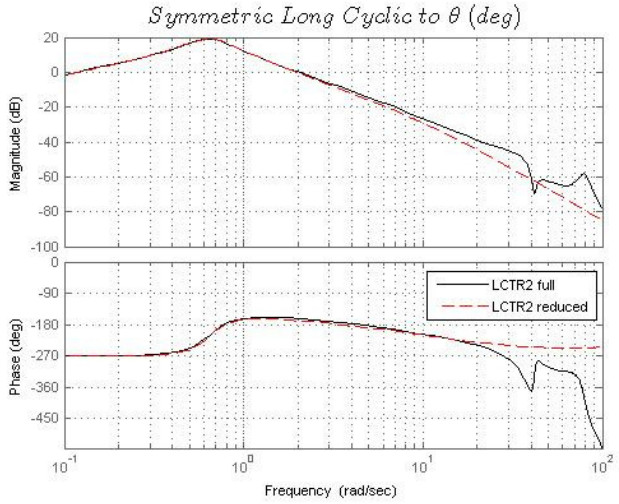


**Figure 3: Comparison of the frequency response of the pitch and roll rate to stick inputs of the CAMRAD II full and reduced order linear LCTR2 models**

Figure 3 shows an example of the frequency response comparison of the full order and reduced order models. The input convention used is based on a plane of symmetry in the aircraft body axes X-Z plane. Symmetric inputs are mirror images of each other in that plane and vice-versa for the anti-symmetric. It can be seen that the dynamics are the same up to a frequency of 10 rad/s, which is sufficient for capturing dynamics for real-time simulation and handling qualities analysis.

This model reduction process was applied to a matrix of CAMRAD II models trimmed at speeds at 20 knot intervals between 0-60kts and for nacelle angles at 95, 90, 75 and 60 degrees. This defines the envelope of the lookup tables for the qLPV model. If the simulation were to attain a flight condition outside the envelope, then the lookup table outputs would limit at the nearest table boundary values.

The selection of the qLPV architecture brought a number of benefits. Firstly, LPV models provide an ability to represent a wider flight envelope whilst retaining the stability derivative model basis. Secondly, the qLPV model is a direct evolution of the 'single-point' linear state-space models used in the previous VMS experiments. This is because it is derived from the same baseline nonlinear model and thus provides a continuity of the models.

### *3.3 IMPLICIT VS. EXPLICITLY MODELED EFFECTS*

It was described earlier that the endogenous scheduling parameters confer special rules in the qLPV model architecture. This is described in detail by the authors of Ref [7] who establish that for states of this nature in a qLPV model, the effect due to their change is implicit in the model, and the equivalent explicit stability derivatives must be eliminated from the model. In brief, the following will explain using an example where if $V_0$ is a scheduled parameter then all u ($M_u$, $Z_u$ etc) derivatives must be = 0. $V_0$ is considered approximately equivalent to **u**, the body axis velocity. The following derivation follows as presented by Zivan and Tischler [7] and is included to support the subsequent analysis. First, consider the standard 1st order Taylor series expansion of the linearized pitching moment equation in trimmed flight for a simplified 6-Dof model with a pure longitudinal control effect due to longitudinal cyclic, $\theta_{1s}$.

$$\begin{aligned}\dot{q} = 0 = M_u\Delta u + M_w\Delta w + M_q\Delta q \\ + M_v\Delta v + M_p\Delta p + M_r\Delta r + M_{\theta_{1s}}\Delta\theta_{1s}\end{aligned} \quad \textbf{(4)}$$

Rearranging this expression to solve for $M_u$:

$$M_u = -\left[\begin{aligned} & M_w\frac{\Delta w}{\Delta u} + M_q\frac{\Delta q}{\Delta u} + M_v\frac{\Delta v}{\Delta u} \\ & + M_p\frac{\Delta p}{\Delta u} + M_r\frac{\Delta r}{\Delta u} + M_{\theta_{1s}}\frac{\Delta\theta_{1s}}{\Delta u}\end{aligned}\right] \quad \textbf{(5)}$$

Note that: $\dfrac{\partial\overline{M}}{\partial u} = M_u = \dfrac{\partial M}{\partial u}\left(\dfrac{1}{I_{yy}}\right)$

Now, the same trim expression is derived for the qLPV model equation – note that the *u* derivative terms have been eliminated:

$$\begin{aligned}\dot{q} = M_w(w-w_0) + M_q(q-q_0) \\ + M_v(v-v_0) + M_p(p-p_0) \\ + M_r(r-r_0) + M_{\theta_{1s}}(\theta_{1s}-\theta_{1s_0})\end{aligned} \quad \textbf{(6)}$$

Here, it is important to remember that the qLPV model approach is to subtract the 'looked-up' trim state ($w_0$ etc) from the value of the absolute state before multiplying by the appropriate derivative so that $\Delta w = (w - w_0)$ etc. With $\dot{q} = \dfrac{M}{I_{yy}} = \overline{M}$ the partial derivative of this expression with respect to $u$ is evaluated to produce the equivalent expression for the derivative:

$$\frac{\partial \overline{M}}{\partial u} = -M_w \frac{\partial w_0}{\partial u} - M_q \frac{\partial q_0}{\partial u} - M_v \frac{\partial v_0}{\partial u} - M_p \frac{\partial p_0}{\partial u} - M_r \frac{\partial r_0}{\partial u} - M_{\theta_{1s}} \frac{\theta_{1s_0}}{\partial u} \quad (7)$$

Comparing equations 5 and 7 shows that effectively the same expression is returned – affirming the premise that the effect due to a change in $u$ is implicit if the model uses flight speed as a scheduling parameter. Note that the ratio terms in equation 7, $\frac{\partial w_0}{\partial u}$ etc, are the slopes of the trim states with respect to the scheduling variable, i.e. $V_0 \cong u$. An assessment of the implicit effect can be carried out by comparing the derivative terms computed by the original numerical perturbation linearization scheme to the equivalent term computed from an expression such as equation 7. The approach requires the local slope to be computed with respect to the particular scheduling variable for each of the model states from the trim maps and then to be multiplied by the appropriate derivative. An example result of the analysis is illustrated in figure 5 which shows the comparison numerical calculation of the implicit derivative to the directly extracted value for the derivative $Z_\beta$.

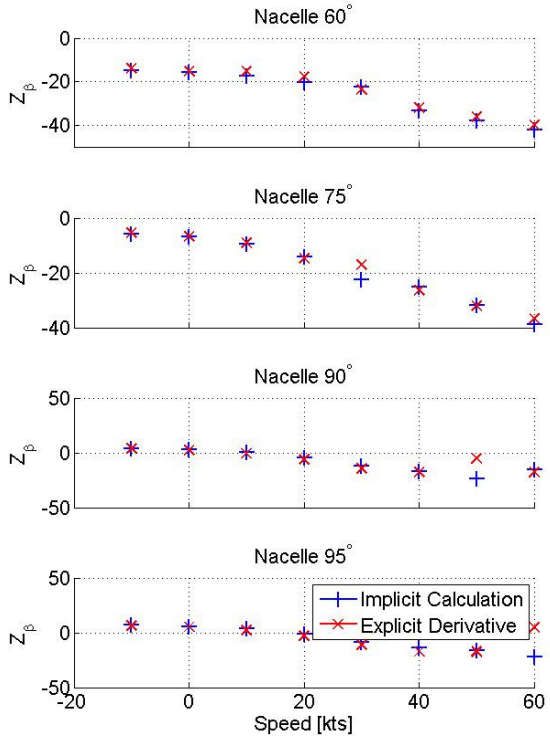


**Figure 4: Comparison of implicitly calculated derivative versus directly extracted derivative for Nacelle ($\beta_m$) perturbation effects**

The results show that the calculation of the implicit value produces a reasonably consistent comparison with the equivalent directly extracted values. There are some mismatches – some of which can be attributed to the fairly crude calculation of the local trim slope used for this comparison.

Overall, the results support the premise in ref [7] that these terms are accounted for implicitly by the combined effect of the trim datum states moving with the changing lookup parameter ($V$, $\beta_m$) and that any stability derivatives with respect to these states/parameters should be eliminated.

### *3.4 ANALYSIS OF THE QLPV ARCHITECTURE*

In order to assess the performance of the qLPV model, comparisons were made to a full non-linear model of the same aircraft. In support of the primary development using derivatives from the CAMRAD II non-linear model, another LCTR2 model was constructed in the FLIGHTLAB modeling environment [10]. Although initially built to provide a 'rapid-prototyping' model to provide stability derivatives for the development of the qLPV model and understanding nacelle dynamics, it has also proved very useful for performing comparisons of the source non-linear model to the qLPV model derived from it. The FLIGHTLAB model was designed to comprise a similar level of modeling fidelity as the baseline CAMRAD II model and the following bullets list its key features:

- Finite element elastic beam blades with 5 structural segments and 5 aerodynamic blade element rotors. Quasi-steady airfoil data with data for changing blade section along radius.
- Finite state inflow model with interference effects to rotor and wing, empennage surfaces.
- Rigid fuselage model with mass and moment of inertia properties.
- Dynamically controllable tilting nacelles
- Segmented lifting-line wing model with a 'horseshoe-vortex' induced inflow model and wake effects to empennage. Wing also features outer panels that tilt with the nacelle angle.
- Simple mechanical gearing control system
- Idealized engine (constant rotor speed).

A key item is that the model featured nacelle control as dynamically controllable input, not just a trim configuration parameter thus allowing extraction of stability derivatives for those model dynamics.

Figure 5 shows a number of frequency response comparisons of the two qLPV models derived from the CAMRAD II and FLIGHTLAB models at hover. Both qLPV models are reduced-order (13 states as is the single point, hover condition linear model derived from CAMRAD II that has been included for comparison. The frequency responses are based on linear models extracted from the qLPV model using perturbation methods. On the whole, the comparisons are satisfactory within the key region of interest (1-10 rad/sec) exhibiting the best agreement for both the rigid-body and rotor responses. These results gave reasonable confidence that conclusions from analysis of the FLIGHTLAB qLPV model would be also applicable to the CAMRAD II based qLPV model.

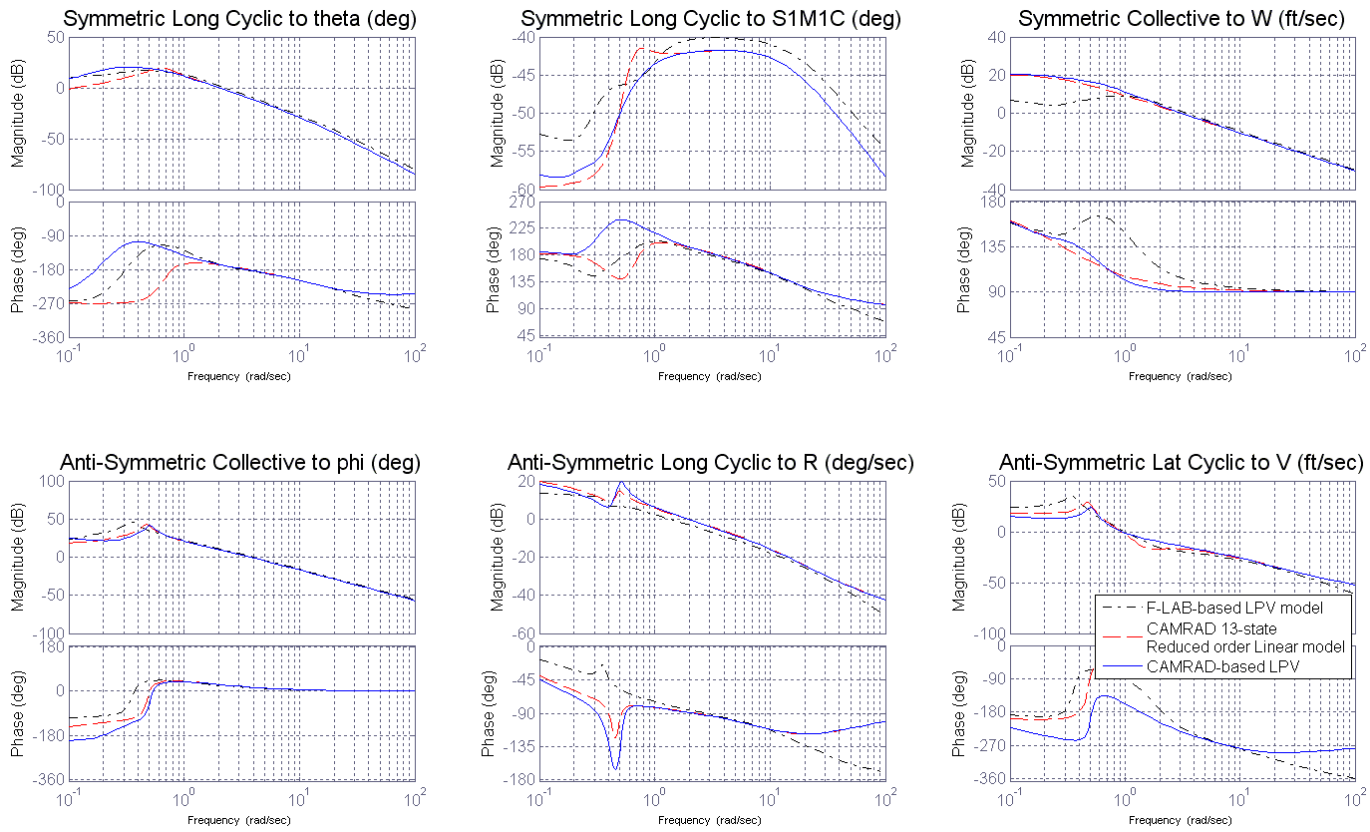


**Figure 5: Comparison of the CAMRAD derived qLPV model (baseline), to the CAMRAD reduced order (13-state) linear model and the FLIGHTLAB derived qLPV model (all at hover condition)**

## 4. NACELLE DYNAMICS AND MODELING

One of the key requirements for the model was the representation of dynamics due to nacelle motions. A single linear model would only be capable of representing effects due to small perturbations of nacelle but the larger nacelle angles demanded by the Depart/Abort MTE exceed the region of validity for such a model. For a tiltrotor, the nacelle is a control as well as a reconfiguration of the aircraft. As such, nacelle motions not only generate forces and moments directly in response to pilot inputs but they also change the dynamics of the vehicle through the reorientation of the rotors in the aircraft body frame.

For the qLPV model derived from the baseline CAMRAD II model, the stability derivatives were extracted for various trim conditions of varying speed and nacelle angles. However, it was also required to calculate the derivatives with respect to the motion of the nacelles themselves. Two options to obtain these parameters were considered, either to extract derivatives from the FLIGHTLAB non-linear model described in section 2, or to analytically compute derivatives from the existing CAMRAD II model derivatives and trim output data. Both had attractions, those derived from the FLIGHTLAB non-linear model were generated through an automated process that implicitly included all effects featured in the multi-body dynamics model.

Whereas the analytical terms, based on first principles, offered an independent process which derived the terms from the same model that the other derivatives were extracted. Although the analytical process omitted certain effects to make the definition and calculation of the terms more tractable, it also provided useful physical insight to the nacelle effects as well as a dataset with which to cross-verify the FLIGHTLAB derivatives.

The following expressions, in vector form, define the full non-linear equations that describe the forces and moments acting on the airframe – nacelle system:

$$\vec{F} = m\vec{a} + m\{S(\vec{\omega})\}\cdot\vec{V} - m_N\left\{S\left(\vec{r}_{N/F}\right)\right\}\cdot\vec{\alpha} + \underline{m_N\{S(\vec{\omega})\}\cdot\{S(\vec{\omega})\}\cdot\vec{r}_{N/F}} + \underline{2m_N\{S(\vec{\omega})\}\cdot\left(\frac{d\vec{r}_{N/F}}{dt}\right)_B} + m_N\left(\frac{d^2\vec{r}_{N/F}}{dt^2}\right)_B \quad \textbf{(8)}$$

$$\vec{M} = \{I\}\vec{\alpha} + \{S(\vec{\omega})\}\cdot\{I\}\vec{\omega} + m_N\left[\left\{S\left(\vec{r}_{N/F}\right)\right\}.\vec{a} + \{S(\vec{\omega})\}\cdot\left\{S\left(\vec{r}_{N/F}\right)\right\}.\vec{V}\right] + \left\{I_{N/F}\right\}\vec{\alpha}_{N/F} + \underline{\{S(\vec{\omega})\}\cdot\left\{I_{N/F}\right\}\vec{\omega}_{N/F}} - \dot{\beta}_m\left[\underline{\frac{d\{I\}}{d\beta_m}.\vec{\omega}} + \underline{m_N\frac{d\left\{S\left(\vec{r}_{N/F}\right)\right\}}{d\beta_m}\cdot\vec{V}} + \underline{\frac{d\left\{I_{N/F}\right\}}{d\beta_m}\vec{\omega}_{N/F}}\right] \quad \textbf{(9)}$$

These equations show that the forcing terms on the left, which are the forces and moments due to aerodynamic, propulsive, mechanical systems, are balanced by the inertial loads generated due to the motions of the fuselage and nacelle masses as a total system as well as mutually relative motions. Note that these expressions have been formulated with the body axis reference frame fixed at a location that is coincident with the fuselage center of mass. In this sense, $\vec{a}, \vec{V}, \vec{\alpha}$ and $\vec{\omega}$ represent the linear and angular accelerations and velocities at that location. The importance of this distinction is that simulation models typically use a fixed point of reference and if the expressions were formulated for a reference frame located at the center of gravity there would be terms that induce relative rotations of the fuselage and nacelle systems with respect to that body reference frame. This is not practicable as the stability derivative terms are only compatible with states that are expressed in a fuselage-body-fixed frame.

The left-hand-side forcing terms, when linearized, and using the assumption of small perturbations, are formulated as a Taylor series of linear analytic functions of the state and control variables. For example, for the Z- force:

$$\delta Z = \sum_{i=1}^{n} \frac{\partial Z}{\partial x_i}.\delta x_i + \sum_{j=1}^{p} \frac{\partial Z}{\partial u_j}.\delta u_j + \frac{\partial Z}{\partial \beta_m}.\delta \beta_m + \frac{\partial Z}{\partial \dot{\beta}_m}.\delta \dot{\beta}_m + \frac{\partial Z}{\partial \ddot{\beta}_m}.\delta \ddot{\beta}_m \qquad \textbf{(10)}$$

Where $Z = Z_0 + \delta Z$ and $x_i$ and $u_j$ respectively indicate the *i*-th state and *j-th* control variables. Similar general expressions can be established for the other body axes forces, moments and rotor blade modal functions. These include the partial derivatives for the nacelle conversion degrees of freedom $\beta_m, \dot{\beta}_m$ and $\ddot{\beta}_m$. Figure 6 illustrates the conventions used for the following derivations, note in particular that a negative nacelle angle, $\beta_m$, is a forward rotation.

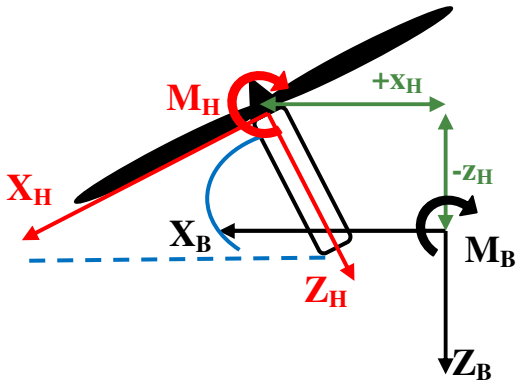


**Figure 6: Axes conventions for nacelle force and moment derivations**

For brevity, only the longitudinal effects are presented, these are by far the most important for the symmetrical longitudinal nacelle motions. The following expressions show how the rotor/nacelle forces in the hub frame are transformed to the body axis reference frame– note that the forces and moments in the hub frame can themselves be a function of the nacelle angle. The following derivations are for a single rotor/nacelle combination so any longitudinal terms are doubled for a two rotor system.

$$X_B = X_H(\beta_m)cos\beta_m + Z_H(\beta_m)sin\beta_m \qquad \textbf{(11)}$$

$$Z_B = -X_H(\beta_m)sin\beta_m + Z_H(\beta_m)cos\beta_m \qquad \textbf{(12)}$$

Applying a small perturbation approach to the Z-force equation results in:

$$\delta Z_B = -\delta X_H sin\beta_m + \delta Z_H cos\beta_m - (X_H cos\beta_m + Z_H sin\beta_m)\delta\beta_m \qquad \textbf{(14)}$$

Now substituting equation 10 into 14 and performing the same with the equivalent expression for $\delta X_H$, the following is obtained:

$$\delta Z_B = \left[\sum_{i=1}^{n} \frac{\partial Z_H}{\partial x_i}.\delta x_i + \sum_{j=1}^{p} \frac{\partial Z_H}{\partial u_i}.\delta u_j\right] cos\beta_m - \left[\sum_{i=1}^{n} \frac{\partial X_H}{\partial x_i}.\delta x_i + \sum_{j=1}^{p} \frac{\partial X_H}{\partial u_j}.\delta u_i\right] sin\beta_m + \left[\frac{\partial Z_H}{\partial \beta_m} cos\beta_m - \frac{\partial X_H}{\partial \beta_m} sin\beta_m - (X_H cos\beta_m + Z_H sin\beta_m)\right]\delta\beta_m + \left[\frac{\partial Z_H}{\partial \dot{\beta}_m} cos\beta_m - \frac{\partial X_H}{\partial \dot{\beta}_m} sin\beta_m\right]\delta\dot{\beta}_m + \left[\frac{\partial Z_H}{\partial \ddot{\beta}_m} cos\beta_m - \frac{\partial X_H}{\partial \ddot{\beta}_m} sin\beta_m\right]\delta\ddot{\beta}_m \qquad \textbf{(15)}$$

Now the partial derivatives with respect to $\beta_m, \dot{\beta}_m$ and $\ddot{\beta}_m$ are made thus obtaining the expressions for the individual stability derivatives:

$$\frac{\partial Z_B}{\partial \beta_m} = \left[-\frac{\partial X_H}{\partial \beta_m} sin\beta_m + \frac{\partial Z_H}{\partial \beta_m} cos\beta_m - (X_H cos\beta_m + Z_H sin\beta_m)\right] \qquad \textbf{(16)}$$

$$\frac{\partial Z_B}{\partial \dot{\beta}_m} = \left[-\frac{\partial X_H}{\partial \dot{\beta}_m} sin\beta_m + \frac{\partial Z_H}{\partial \dot{\beta}_m} cos\beta_m\right] \qquad \textbf{(17)}$$

$$\frac{\partial Z_B}{\partial \ddot{\beta}_m} = \left[-\frac{\partial X_H}{\partial \ddot{\beta}_m} sin\beta_m + \frac{\partial Z_H}{\partial \ddot{\beta}_m} cos\beta_m\right] \qquad \textbf{(18)}$$

Finally, the analytic expressions for the calculation of the partial derivative terms such as $\frac{\partial X_H}{\partial \dot{\beta}_m}$, $\frac{\partial X_H}{\partial \ddot{\beta}_m}$ etc on the right-hand-side of the previous equations need to be defined. These terms are the change of the rotor hub frame forces

with respect to the nacelle dynamics. Again, focusing on the Z-force term, the variation due to the nacelle angle, $\beta_m$, can be approximated using momentum theory.

The simplifying assumptions that permit the use of this analytical approach are that the airspeeds are low (incompressible), angles of attack remain small (within the linear regime) and that rotorspeed remains constant. All other conditions remaining constant, nacelle perturbations are analogous to changes in angle of attack of the rotor, $\delta\beta_m = \delta\alpha$. Making the approximation $-Z_H = T$, the analytical expression of the rotor hub Z-force based on the assumption of uniform constant inflow is:

$$Z_H = -\frac{N_b \rho C_{l_\alpha} \Omega^2 \mathrm{R}^3 \mathrm{c}}{2} \times \quad \textbf{(19)}$$

$$\left[\left(\frac{1}{3}+\frac{\mu_x^2}{2}\right)\theta_0 + \left(\frac{1}{4}+\frac{\mu_x^2}{4}\right)\theta_{tw} + \frac{\mu_x}{2}\theta_{1s} - \frac{\lambda_i}{2} + \frac{\mu_z}{2}\right]$$

Again using linear theory, a small perturbation in $Z$ is:

$$\delta Z_H = -Z_H \quad \textbf{(20)}$$

$$\frac{\left(\mu_x\theta_0 + \frac{\mu_x}{2}\theta_{tw} + \frac{1}{2}\theta_{1s}\right)\mu_z - \frac{\mu_x}{2}}{\left(\frac{1}{3}+\frac{\mu_x^2}{2}\right)\theta_0 + \left(\frac{1}{4}+\frac{\mu_x^2}{4}\right)\theta_{tw} + \frac{\mu_x}{2}\theta_{1s} - \frac{\lambda_i}{2} + \frac{\mu_z}{2}} . \delta\alpha$$

Such that the partial derivative with respect to $\beta_m$ becomes:

$$\frac{\partial Z_H}{\partial \beta_m} = -Z_H \times \quad \textbf{(21)}$$

$$\frac{\left(\mu_x\theta_0 + \frac{\mu_x}{2}\theta_{tw} + \frac{1}{2}\theta_{1s}\right)\mu_z - \frac{\mu_x}{2}}{\left(\frac{1}{3}+\frac{\mu_x^2}{2}\right)\theta_0 + \left(\frac{1}{4}+\frac{\mu_x^2}{4}\right)\theta_{tw} + \frac{\mu_x}{2}\theta_{1s} - \frac{\lambda_i}{2} + \frac{\mu_z}{2}}$$

It is noteworthy to mention that for the hover case, this term is zero, as would be the similar expression for the rotor hub X-force derivative. As such, the derivative in the body frame from equation 16 simply becomes the underlined term, which is actually equal to the negative of trim X-force (equation 11). This demonstrates that for small angles at hover, the perturbation forces due to nacelle angle changes are approximated to the quasi-steady reorientation of the hover trim forces.

A similar process can be carried out for the remaining force and moments in the other axes – for the case of the X-force and pitching moment, *M*, the expressions are somewhat more complicated, whereas if symmetrical flight and rotor symmetry is enforced, the lateral terms become simplified. The remaining effects due to nacelle conversion rate $(\delta\dot{\beta}_m)$ can be approximated using the existing rotor flapping derivatives with respect to body motions by using the analogy of nacelle rate to body pitch rate.

Table 1 shows a comparison of the stability derivatives extracted from the FLIGHTLAB model and the analytical calculations. This example is at the hover condition with the nacelles at the 90 degree (vertical) position. The agreement between this case and others not presented gave reassurance that automatic derivative calculation process from FLIGHTLAB was providing reliable results.

| | **FLIGHTLAB** | **Analytical** |
|---|---|---|
| $\frac{\partial X_B}{\partial \beta_m}$ | -34.2 | -34.8 |
| $\frac{\partial Z_B}{\partial \beta_m}$ | 2.39 | 1.87 |
| $\frac{\partial M_B}{\partial \beta_m}$ | 0.0514 | 0.035 |
| $\frac{\partial \beta_{1c}}{\partial \dot{\beta}_m}$ | 1.24 | 0.955 |
| $\frac{\partial X_B}{\partial \ddot{\beta}_m}$ | 0.272 | 0.264 |
| $\frac{\partial M_B}{\partial \ddot{\beta}_m}$ | -0.0139 | -0.0253 |

**Table 1: Comparison of nacelle stability derivatives extracted from the FLIGHTLAB LCTR2 model and analytical technique (trim: hover, 90deg nacelle)**

The earlier availability of the analytical derivatives led to their use in the TRC control design process. This did not cause significant problems when the controller was applied to the qLPV model that featured the more complete set of FLIGHTLAB nacelle motion derivatives. This similarity of the dynamic response is illustrated in Figure 7, which shows the frequency response of the longitudinal velocity to the nacelle angle input for the two derivative sets.

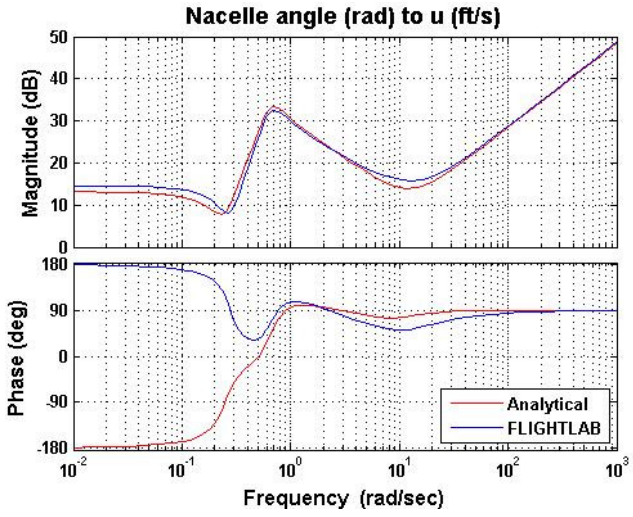


**Figure 7: Comparison of frequency responses of nacelle input to aircraft u velocity using FLIGHTLAB and Analytical derivatives**

This validation against the analytical approach led to the use of the FLIGHTLAB automatically generated derivatives in the final qLPV model. These were added as additional columns (only $\dot{\beta}_m$ and $\ddot{\beta}_m$ explicit derivatives were required

as explained in section 3.3) in the **B** matrix and were implemented as functions of lookup parameters.

## 5. CONTROL SYSTEM IMPLEMENTATION AND INTEGRATION WITH QLPV MODEL

### *5.1 ACAH CONTROL LAWS*

The complete bare airframe qLPV model, including nacelle dynamics, was integrated into a model-following control system architecture as shown in Figure 8.

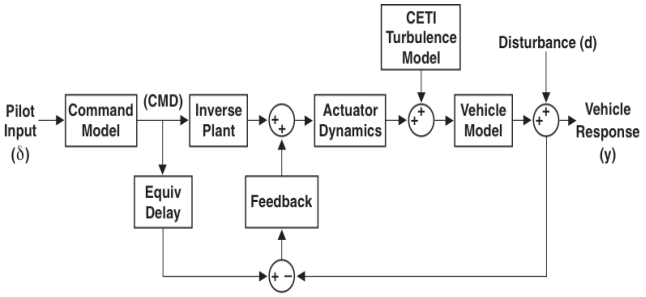


**Figure 8: Overview of the model-following control system architecture**

The control system augments the aircraft response to provide Attitude Command, Attitude Hold (ACAH) response types in pitch and roll and Rate Command (RC) in yaw. Further details on the controller and its performance can be found in references [3] and [4]

The key additions required with the introduction of the qLPV model were modules to provide nacelle actuation dynamics (angle rate and acceleration), a lateral and longitudinal translation rate control system, and algorithms to trim and initialize the bare airframe qLPV model combined with the control system.

### *5.2 NACELLE ACTUATION AND TRC*

The new qLPV bare-airframe model provided the additional dynamics but additional control law and actuator models were required to represent various means of controlling the parallel lateral cyclic and nacelle tilt in manual and TRC modes.

The nacelle dynamics themselves were modeled as a second order system with an idealized natural frequency and damping ratio that provided a representation of angle, rate and acceleration dynamics without causing oscillations or interference with the fundamental aircraft dynamics.

The baseline nacelle control input was a discrete-step, 'beep' control, with stop points at angles of 95, 86, 75 and 60 degrees (the 75 deg stop is replaced by a 80deg one when approaching the from a smaller angle (i.e. returning towards hover position). Here the pilot pushes a rocker switch fore or aft to step the nacelle angle either forwards or backwards to the next stop angle at a constant angular rate - this approach has been successfully applied on previous research tiltrotors such as the XV-15 [12]. Additionally, a control system for the pilot to continuously command nacelle angular rate was implemented where the rate was proportional to inceptor position. In terms of actuator dynamics the nacelles are limited to an aft position of 95 degrees and forwards to 0 degrees in all modes. For the discrete beep and direct angular rate mode the nacelle actuation rates are limited as in Table 2, with values based on those typically used in prior research at NASA.

| Discrete 'Beep' Mode | | Direct rate command |
|---|---|---|
| >60 deg | ±2 deg/s | ±7.5 deg/s throughout range |
| <60 deg | ±3 deg/s | |

**Table 2: Nacelle conversion rate limiting in pilot manual control modes**

The TRC control laws followed the same architecture as the ACAH control laws in that it consisted of a feedforward command model and a feedback regulator part that closes the loop on the commanded translational velocities. The TRC mode uses the nacelles to control longitudinal velocity. The model is designed such that the nacelle actuator rate and angular limits can be varied to explore what implications there are on the handling qualities using this control method. The lateral velocity is controlled using lateral parallel cyclic on both rotors. The TRC is primarily aimed at improving the handling qualities in the precision hover task and therefore the velocity range it commands is approximately ±18ft/s (11kts) for a maximum useful input.

In addition to the 'pure' TRC mode where the velocities are commanded whilst the attitudes are held steady, a combined TRC/ACAH control mode was implemented where the pilot inputs commanded velocity and attitude changes simultaneously. This allowed the investigation of pilot preference of the aircraft response in TRC as well as the tradeoff between rotor flapping and attitude response in TRC.

### *5.3 PILOT INCEPTORS*

In addition to the various control modes, different inceptor options were made available for experimentation. For the nacelle beep control, a discrete rocker switch on the pilot's Thrust Control Lever (TCL) was provided to for command of the fore/aft tilting of the nacelles between stop points.

Also located on the TCL was a thumb stick that was used for different functions, as illustrated in Figure 9. Without TRC enabled, it was configured such that the fore/aft axis proportionally commanded nacelle angular rate. When in TRC mode, the thumb stick became a two-axis controller commanding the translational velocities in a fore/aft and left/right plane. The stick is sprung such that if it is released, the stick centers and automatically commands zero velocity. An alternative option of commanding the TRC via the center stick was also implemented. This was enabled simply via a mode switch and as its use was to be limited to the Precision Hover MTE it did not require any automatic mode

switching. Also, the previously mentioned combined attitude/TRC control mode was to be controlled only via this center stick method of TRC input.

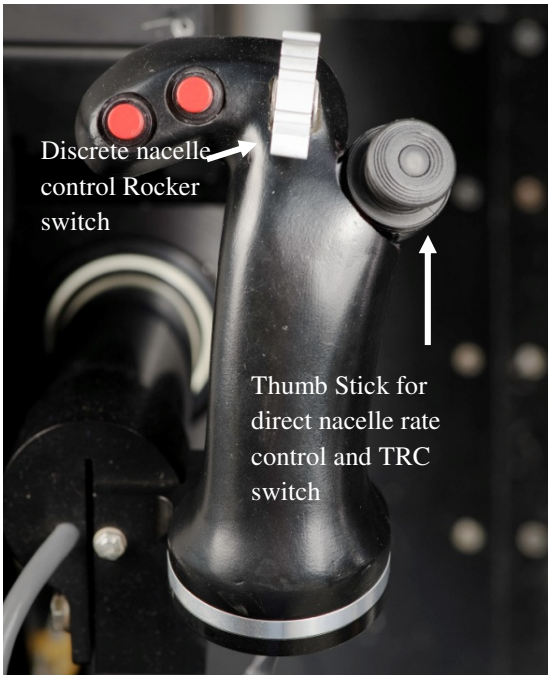


**Figure 9: Rocker Switch and Thumb Stick on Thrust Control Lever in VMS cockpit**

A final development was that the center stick and thumb stick TRC control inceptors were configured to be live simultaneously. This meant that if the center stick TRC mode was active, thumb stick TRC inputs could also be made and the inputs from the two inceptors were additive. This was implemented in response to pilot feedback where exploratory simulations found it to be preferable to use the different inceptors in different phases of the Precision Hover MTE.

## 6. SIMULATION EVALUATION AND DISCUSSION

The combined qLPV airframe and control law models in MATLAB/Simulink were auto coded into an executable library using the Real-time Workshop utility. This version of the model was then integrated into the NASA VMS simulation environment where it could be flown in both fixed- and motion-base simulator environments.

The real-time version of the model was tested extensively by the project pilot in the development and workup phases to the simulation experiments. The pilot comments were that the model was very much similar to the model used in previous experiments [3],[4]. Differences were detected, such as greater couplings (a deliberate addition to the bare-airframe model), which were especially prevalent in the yaw axis response – however these did not change the pilot's assessment of the handling quality ratings in the Precision Hover MTE. More generally, for the limited envelope of hover and low speed, the model was adjudged by the project pilot to be representative of other simulations of small and medium size tiltrotors. The results support the assessment that the new model substantially exhibited the same dynamics and handling qualities as the previous model.

Figure 10 illustrates some of the new capabilities of the model with a time history of the qLPV model being flown in a piloted simulation of a Depart/Abort maneuver. The aircraft starts the in the hover after which the nacelles are tilted forward (<86deg) and the aircraft accelerates forward reaching a maximum speed of ~80ft/s (47kts). Also note during the phase where nacelles are moved to the full aft position (95deg) to initiate the deceleration, the pitch disturbances and associated compensating pilot longitudinal stick inputs.

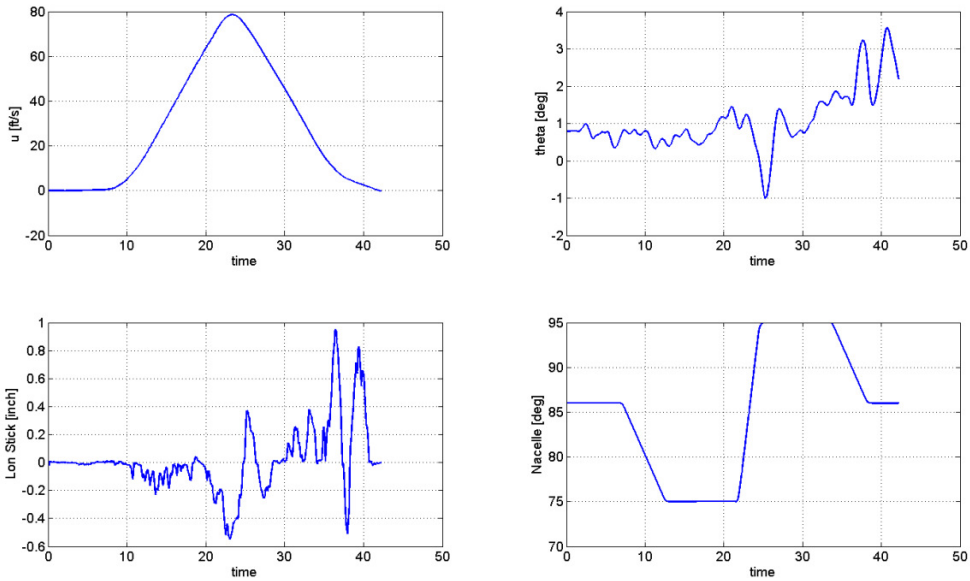


**Figure 10: Time history of qLPV model flown in piloted simulation of Depart/Abort MTE**

## 7. SUMMARY AND CONCLUSIONS

This paper has described how a qLPV modeling approach has been applied to creating a simulation of the NASA Large Civil Tiltrotor. It has been demonstrated that the technique was successfully applied to a tiltrotor model including using multiple dimensional lookup tables of speed and nacelle angles. The premise that a qLPV model implicitly accounts for effects due to perturbations in the scheduling parameters via the trim change data was supported through comparisons with the equivalent stability derivatives that were directly computed

A detailed appraisal of modeling the nacelle kinematics in a qLPV was presented – including a presentation of how stability derivatives representing these effects can be calculated from baseline 6-DoF and rotor flapping derivatives and trim data. The comparison of the results of the two approaches exhibited levels of agreement that cross-verified the analytical and FLIGHTLAB model nacelle motion derivatives. It was also shown that TRC control laws designed using the simple analytical derivative set were successfully applied to the qLPV model that featured the complete set of nacelle derivatives from FLIGHTLAB.

The bare airframe qLPV model was successfully integrated with ACAH model-following control laws and upgraded to feature Translational Rate Control using a combination of nacelle tilting and lateral cyclic inputs. The model was successfully integrated into the NASA Vertical Motion Simulator, several inceptor configurations were implemented for investigation of various methods of tilting nacelles and providing TRC in hover and low speed maneuvering. Piloted testing received favorable comments, with no degradation due to the new model architecture, whilst bringing additional control modes and model dynamics.

Overall, the model was adjudged to be fit for the purpose of the upcoming VMS piloted handling qualities simulation experiments of the LCTR2 in hovering and low speed mission task elements.

## 8. ACKNOWLEDGEMENTS

This research was supported by an appointment to the NASA Postdoctoral Program at the Ames Research Center administered by Oak Ridge Associated Universities through a contract with NASA. Strong recognition must also be given to NASA colleagues Bill Decker and Jim Lindsey, their respective engineering and pilot experience with tiltrotor aircraft was invaluable in supporting the development of this model.

## 9. REFERENCES

[1] Johnson, W., Yamauchi, G.K, Watts, M.E, “NASA Heavy Lift Rotorcraft Systems Investigation”, NASA/TP-2005-213467, NASA Ames Research Center, December 2005.

[2] Acree, Jr., C. W., Yeo, H., and Sinsay, J., Performance Optimization of the NASA Large Tiltrotor, NASA/TM-2008-215359, June 2008.

[3] Blanken, C.L., Lusardi, J.A., Ivler, C. M. Tischler, M.B., Höfinger, M.T., Decker, W.A., Malpica, C.A., Berger, T., Tucker, G.E., “An Investigation of Rotorcraft Stability-Phase Margin Requirements in Hover”, American Helicopter Society 65th Annual Forum, Grapevine, Texas, May 27 - 29, 2009.

[4] Malpica, C.A., Decker, W.A., Theodore, C.R, Blanken, C.L., Berger, T., “An Investigation of Large Tilt-Rotor Short-term Attitude Response Handling Qualities Requirements in Hover”, American Helicopter Society 66th Annual Forum, Phoenix, AZ, May 11-13, 2010.

[5] Anon., "Handling Qualities Requirements for Military Rotorcraft", Aeronautical Design Standard-33 (ADS-33E-PRF), US Army Aviation and Missile Command, March 21, 2000.

[6] Marcos, A., Balas, G.J., “Development of Linear-Parameter-Varying Models for Aircraft”, AIAA Journal of Guidance, Control, and Dynamics, Mar-Apr 2004, 0731-5090 vol.27 no.2 (218-228)

[7] Zivan, L., Tischler, M.B., “Development of a Full Flight Envelope Helicopter Simulation Using System Identification”, Journal of the American Helicopter Society, Vol 55, No. 2, April 2010.

[8] Tischler, M.B., “Aerodynamic Model for Piloted V/STOL Simulation”, Systems Technology Inc (STI) Working Paper 1171-2, March 1982.

[9] Aiken, E.W., “A Mathematical Representation of an Advanced Helicopter for Piloted Simulator Investigations of Control System and Display Variations”, NASA Technical Memorandum TM-81203, July 1980.

[10] DuVal, R. W., “A Real-time Multi-Body Dynamics Architecture for Rotorcraft Simulation”, *The Challenge for Realistic Simulation*, RAeS Conference, London 2001.

[11] McFarland, R.E., “Trimming an Aircraft Model for Flight Simulation”, NASA Technical Memorandum TM-89466, October 1987.

[12] Decker, W.A., Handling Qualities Evaluation of XV-15 Noise Abatement Landing Approaches Using a Flight Simulator. Presented at the American Helicopter Society 57th Annual Forum, Washington, DC, May 9-11, 2001.